scientific reports

Check for updates

OPEN

Nonadiabatic dynamics of cobalt tricarbonyl nitrosyl for ligand dissociation induced by electronic excitation

Yeonghun Lee[1], **Grigory Kolesov**[2], **Xiaolong Yao**[1], **Efthimios Kaxiras**[2,3] & **Kyeongjae Cho**[1]✉

We utilize real-time time-dependent density functional theory and Ehrenfest dynamics scheme to investigate excited-state nonadiabatic dynamics of ligand dissociation of cobalt tricarbonyl nitrosyl, $Co(CO)_3NO$, which is a precursor used for cobalt growth in advanced technologies, where the precursor's reaction is enhanced by electronic excitation. Based on the first-principles calculations, we demonstrate two dissociation pathways of the NO ligand on the precursor. Detailed electronic structures are further analyzed to provide an insight into dynamics following the electronic excitations. This study sheds light on computational demonstration and underlying mechanism of the electronic-excitation-induced dissociation, especially in molecules with complex chemical bonds such as the $Co(CO)_3NO$.

The scaling limit for the current complementary metal–oxide semiconductor (CMOS) technology necessitates a three-dimensional integration with vertically stacked electronic components[1]. This requires low thermal budget processes in order to prevent the degradation of devices and interconnects underneath the top layer undergoing thermal processes. Electron-enhanced atomic layer deposition (EE-ALD) can be a solution to create reactive dangling bonds at low temperatures by using an energetic electron beam[2–4]. In addition to the EE-ALD, the energetic electrons can be exploited for focused electron beam induced deposition (FEBID), which is a useful technique for nanopatterning on solid surfaces[5]. Cobalt has been paid a lot of attention as a promising interconnect material. The continuous increase in the density of transistors keeps reducing the metal interconnect width. However, further scaling of current copper and tungsten interconnects is challenging due to their requirement of a thick diffusion barrier, which brings about a narrow conductive cross-sectional area. This limitation becomes rapidly severe as scale decreases. To overcome the issue, barrierless cobalt can be a promising interconnect material to replace the copper and tungsten[6]. Also, cobalt enables us to pattern FEBID nanostructures for catalytic and ferromagnetic applications[7,8]. Here, a widely used organometallic cobalt precursor is cobalt tricarbonyl nitrosyl, $Co(CO)_3NO$[4,9,10]. The high metal content of this compound is associated with low incorporation of impurities, such as C, N, and O, resulting in high conductivity.

The electron-induced dissociation of ligands on the Co(CO)3NO has been investigated experimentally in gas phase[11–14] or in liquid helium nanodroplets[15]. A reaction of the gas phase Co(CO)3NO can mimic that on an inert oxide surface. This corresponds to the initial stage of a cobalt film deposition, which is typically slow and requires to be accelerated. The electron-induced dissociation occurs once energy is transferred from the energetic electrons to the target via inelastic electron scattering processes. Photodissociation also involves the pertinent excitation-driven phenomenon, where excitation is introduced in internal degrees of freedom of the molecule. The photodissociation of ligands on the $Co(CO)_3NO$ has also been studied in previous experimental works[16–20]. While experimental progress based on such excitation-induced dissociation of the $Co(CO)_3NO$ has been actively reported in terms of relatively long-time processes by taking into account intramolecular vibrational energy redistribution, there have been very few theoretical studies providing microscopic insights on the process. Specifically, a direct ligand dissociation pathway has not yet been demonstrated, and the first-principles dynamics simulation can play a role in elucidating the ultrafast phenomenon.

This work elucidates the atomic and electronic processes that constitute the excitation-driven dissociation of ligands on $Co(CO)_3NO$ using the first-principles calculation based on the density functional theory (DFT)[21,22].

[1]Department of Materials Science and Engineering, University of Texas at Dallas, Richardson, TX 75080, USA. [2]John A. Paulson School of Engineering and Applied Sciences, Harvard University, Cambridge, MA 02138, USA. [3]Department of Physics, Harvard University, Cambridge, MA 02138, USA. ✉email: kjcho@utdallas.edu

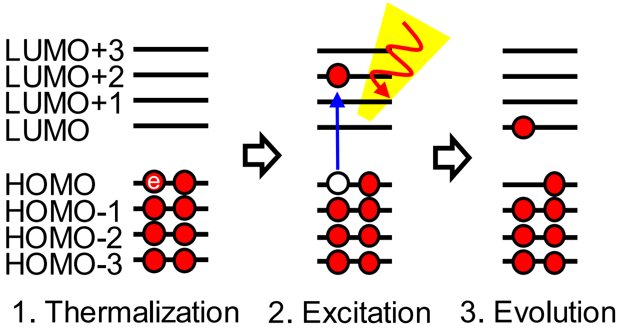

Figure 1. Sequence of TDDFT-MD modeling of reaction induced by electronic excitation.

The molecular dynamics (MD) within the Born–Oppenheimer approximation[23], however, cannot describe such nonadiabatic dynamics along with electronic excitation. To deal with nonadiabatic processes in the coupled electron–ion systems, we employ the real-time time-dependent density functional theory (TDDFT)[24,25] and Ehrenfest dynamics scheme[26–29]. In the present study, we locate direct dissociation channels, thus providing an insight into the excitation-driven unimolecular dissociation of the $Co(CO)_3NO$.

Methods

TDDFT-MD simulation. To explore excited-state nonadiabatic dynamics, we carry out ab initio molecular dynamics study employing the TDDFT-MD based on Ehrenfest dynamics, which has been implemented in a computational package, TDAP-2.0 (Time-evolving Deterministic Atom Propagator)[28–32] based on the SIESTA[33] package. The exchange–correlation (XC) energy functional is given by the Perdew-Burke-Ernzerhof (PBE) functional[34] in the generalized gradient approximation (GGA), and the adiabatic approximation[25] is employed for the XC functional in the TDDFT. The GGA functional is a reasonable choice not only to reproduce experimental measurements[35] but also to maintain consistency with TDDFT works based on pure DFT methods. The norm-conserving pseudopotentials are constructed with Troullier–Martins scheme[36]. A localized, atom-centered, numerical atomic-orbital basis set is employed. We use the double-ζ polarized (DZP) basis set configuration and perform spin-polarized calculations. The real-space mesh cutoff is 120 Ry, and we use 13 Å × 13 Å × 13 Å simulation cell. Convergence tolerance of the density matrix is set to 10^{-4}. The time step for integration is 0.5 ħ/Ry (1 Hartree a.u.)[28,32,37,38], which is reliable as we did not observe any divergence in physical observables. We have performed a convergence test with different mesh cutoffs, resulting in the 120 Ry of the mesh cutoff exhibits enough convergence in the total energy. We have also tested single-ζ polarized (SZP) basis set, where the SZP shows the same key features as the DZP in time-evolving Co-X bond lengths with different excitations. Therefore, the larger DZP basis set would be a safe choice. We note that a dipole correction should be employed to eliminate the spurious electric field induced by the periodic boundary condition. The artificial electric field accelerates ionic motion, often leading to erroneous dissociation.

In the Ehrenfest dynamics, ions are approximated by classical particles evolving on the mean-field average of adiabatic potential energy surfaces (PESs); thus, detailed balance[39], spontaneous phonon emission[40,41], and zero-point motion[30,40] are missing. As to the $Co(CO)_3NO$, the validity of the Ehrenfest approximation will be discussed in the following section. Furthermore, the adiabatic XC functional depends only on the instantaneous electronic density, neglecting memory effects (time-non-locality), which involve the initial-state dependence and history dependence[25]. Despite these limitations, the Ehrenfest dynamics and the adiabatic XC functional have been utilized widely in most practical applications[28–32,37,38,42–45]. For instance, reaction pathways of photodissociation of water on the rutile $TiO_2(110)$ surface and photo-oxidation of CH_3O on the same surface have been illustrated with the same scheme[29,31].

Protocol of ligand dissociation modeling. Figure 1 illustrates the TDDFT-MD modeling of ligand dissociation driven by electronic excitation. First, at the ground state, geometry is optimized until the maximum force is below the tolerance value of 0.04 eV/Å. Then, equilibration at room temperature is performed with the ground-state Born–Oppenheimer molecular dynamics. After that, an excited state is created using the Δ self-consistent field (ΔSCF) method[46,47], which simulates an electronic excitation induced by an inelastic electron scattering or a photoexcitation. For instance, an electron is promoted from the highest occupied molecular orbital (HOMO) to the third-lowest unoccupied molecular orbital (LUMO + 2), which is followed by orbital relaxation within the ΔSCF method. Finally, we let the excited system evolve in time, where coupled electron–ion dynamics is described by the TDDFT-MD. When extracting static microscopic quantities, the geometry optimized at the ground state is used.

Results and discussion

Electronic structure calculations. In the ground state, the organometallic precursor $Co(CO)_3NO$ has a distorted tetrahedral geometry belonging to the C_{3v} point group with the Co–N–O bond being linear in the axial position (Fig. 2a)[48,49]. First, we analyze the electronic ground state (singlet). Figure 2b shows the density

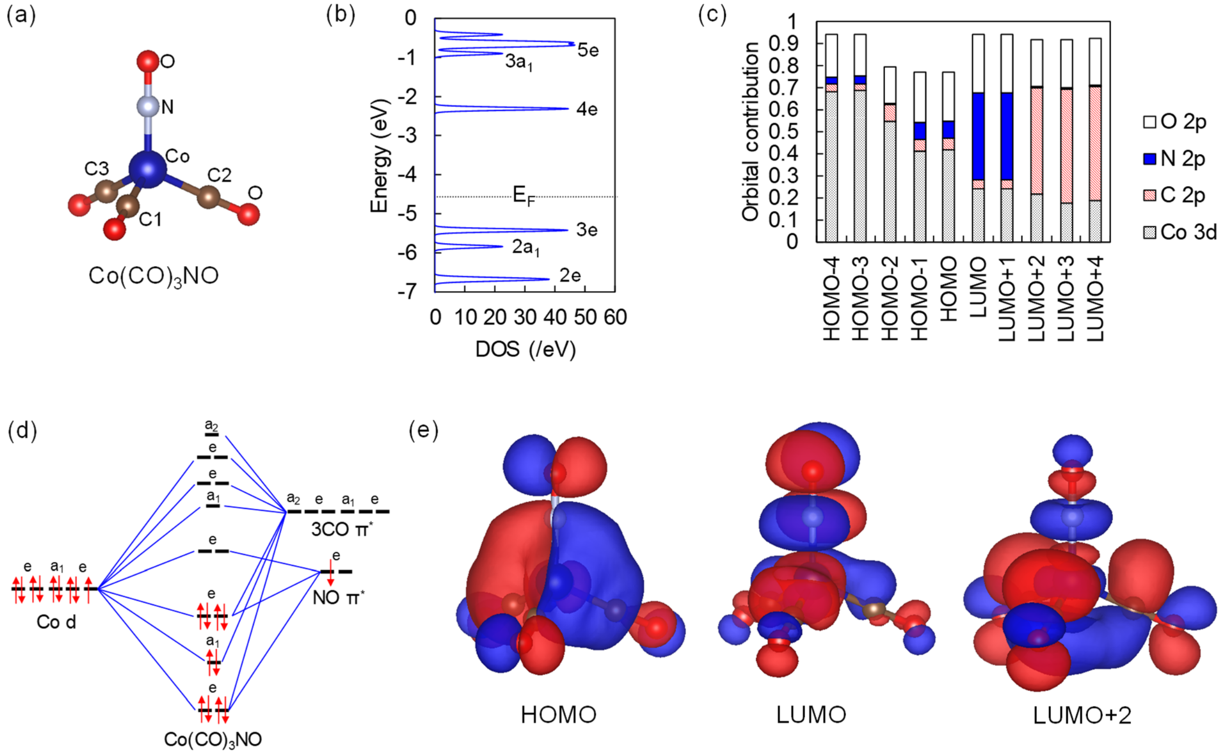

Figure 2. Molecular geometry and electronic structures in the ground state. (**a**) Atomistic structure of $Co(CO)_3NO$. (**b**) DOS around the Fermi level, E_F. (**c**) KS eigenstates decomposed into orbital contributions. (**d**) Molecular orbitals for $Co(CO)_3NO$ with the C_{3v} point group. (**e**) Wavefunction of HOMO, LUMO, and LUMO + 2. Two different colors—blue and red—are assigned to positive and negative isosurfaces.

of states (DOS) around the Fermi level, and Fig. 2c shows contributions of Co 3*d*, C 2*p*, N 2*p*, and O 2*p* orbitals to those energy levels. The orbitals around the Fermi level are described by the metal *d* and ligand π backbond. More specifically, empty π^* orbitals of CO and NO contribute to bonds with Co *d* orbital. The molecular orbital diagram for $Ni(CO)_4$, which has the same number of electrons with the $Co(CO)_3NO$ but has a higher symmetry, helps us to understand where the molecular orbitals of the $Co(CO)_3NO$ originate from. The diagram shown in Figure S1 describes how the π backbond forms in the $Ni(CO)_4$[50]. Compared with the $Ni(CO)_4$, the replacement of a CO group by a NO group changes the point group from T_d into C_{3v} in the $Co(CO)_3NO$ and lifts degeneracies as shown in Fig. 2d. [35]. The HOMO 3*e* orbitals exhibit the π backbond between Co and ligands. Looking at unoccupied states, the LUMO and LUMO + 1 are doubly degenerate 4*e* orbitals, the LUMO + 2 is a nondegenerate $3a_1$ orbital, and the LUMO + 3 and LUMO + 4 are doubly degenerate 5*e* orbitals. The bonding characteristics turn out to be clearer when we analyze the real-space distribution of those wavefunctions. As illustrated in Fig. 2e, the LUMO and LUMO + 1 are an antibonding state formed by Co *d* and the NO π^*-antibonding state, and the LUMO + 2, LUMO + 3, and LUMO + 4 are likewise an antibonding state formed by Co *d* and the CO π^*-antibonding state. We exploit these distinguishing LUMO and LUMO + 2 states to simulate excited-state dynamics for ligand dissociation, where an electron is promoted from the HOMO to the LUMO (3*e* to 4*e*) or from the HOMO to the LUMO + 2 (3*e* to $3a_1$). The excitation operation is done within the same spin channel in such a way that a spin-up (spin-down) electron is promoted to a spin-up (spin-down) empty state. Thus, a sum of singlet and triplet states describes the excitation as usual in a single-determinant approach[51–53].

Standard process driven by single-electron excitation. Figure 3 shows the results of coupled electron–ion dynamics driven by the HOMO-to-LUMO and HOMO-to-LUMO + 2 excitations. Here, ion temperature corresponds to ion kinetic energy, and the electron total energy includes the ion-ion potential energy. During the initial equilibration (from – 100 to 0 fs), the molecule reaches room temperature (Fig. 3a). Then, the excitations are forced at 0 fs, and electron total energies increase abruptly (Fig. 3b). During subsequent dynamics, ion temperature increases up to around 1000 K for both the excitations; at the same time, electron total energy decreases, where the summation of them remains constant. Once the excitations are introduced, the electronic state changes; thus, forces are spontaneously exerted on atoms (Table S1). These exerted forces drive ion vibration followed by electron dynamics. Keeping track of interatomic distances between Co and adjacent atoms, the vibrations are damped, and the initially localized vibrational energy is redistributed eventually (Fig. 3c,d). This indicates that rapid dissociation is unlikely to happen with the given conditions.

Systems with simple σ bonds. We further investigated excited-state dynamics initiated by various excitations in different combinations of unoccupied and occupied molecular orbitals (Table S2) and driven by ioniza-

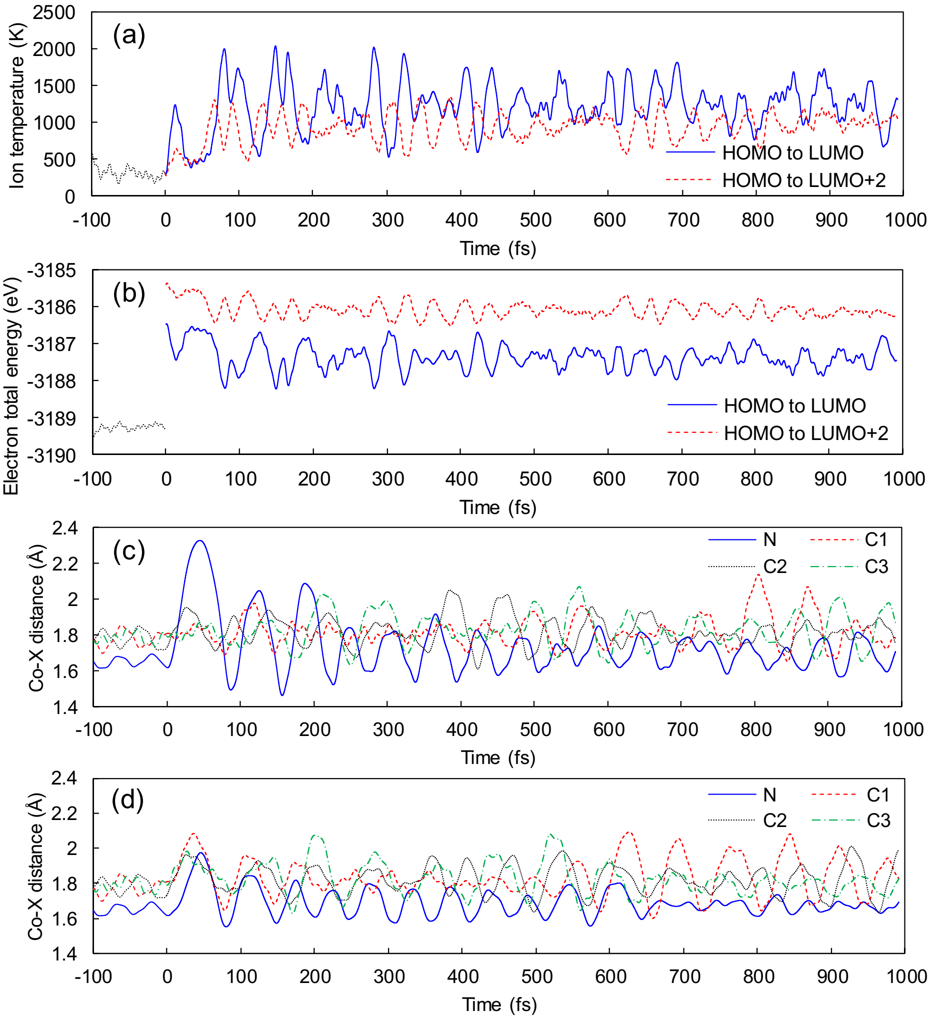

Figure 3. Excited-state dynamics. (**a**) Ion temperature and (**b**) electron total energy as functions of time, where the electron total energy includes ion-ion potential energy. First, systems are equilibrated at 300 K from − 100 to 0 fs; next, HOMO-to-LUMO and HOMO-to-LUMO + 2 excitations are induced at 0 fs; then, the excited states evolve in time from 0 to 1000 fs. Time evolution of Co-X distances induced by (**c**) HOMO-to-LUMO and (**d**) HOMO-to-LUMO + 2 excitations (X = N, C1, C2, C3).

tion and electron attachment (Figure S2). The results revealed that dissociation is unlikely to occur with a single electron process without an additional driving force. The Co–N or Co–C bond is a triple bond consisting of a σ bond and a pair of π backbonds. This complex bonding nature between the metal and ligands prevents dissociation after promoting a single electron. On the other hand, simple σ bonds in H_2, H_2O, and CH_4 facilitate hydrogen dissociation with the HOMO-to-LUMO one-electron excitation (Figure S3a-c). As in $Co(CO)_3NO$, immediate dissociation is unlikely to happen in OCS because four electrons are responsible for each bond by forming σ and π bonds, simultaneously (Figure S3d).

Analysis of time evolution of Kohn–Sham orbital energy levels. For further investigation of electron dynamics, we examine the time evolution of Kohn–Sham (KS) orbital energy levels, which are expectation values of the KS Hamiltonian with respect to time-evolving KS orbitals. Although it is known that the absolute value of KS orbital energy levels hardly possesses physical meaning, relative values provide useful information, such as a transition from an electronically excited state to the ground state, as shown in Fig. 4. Here, the applicability of Kasha's rule[54] and the validity of the Ehrenfest dynamics for the system can be discussed with the transition of the electronic states. Kasha's rule is applicable when energy differences between S_n (nth-excited state) and S_1 are small, and the energy difference between S_0 (ground state) and S_1 is large so that an electronic state can stay at the S_1 for a long time. Figure 4a shows that the lowest excited state, S_1, only lasts for a short time less than 50 fs. Within that time, internal conversion (IC) to the electronic ground state is accompanied by ion dynamics. Since the lifetime of the S_1 is too short for the S_1 to manage molecular dissociation, Kasha's rule would not be applicable to the dissociation dynamics of the $Co(CO)_3NO$. Guo et al.[55] have also been reported such ultrafast IC dynamics in energetic dimethylnitramine, where the lifetime of S_1 is 50 ± 16 fs. When it comes to the

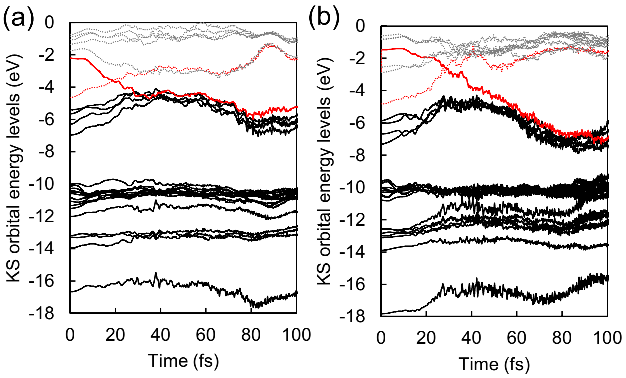

Figure 4. Time evolution of spin-up KS orbital energy levels driven by (**a**) HOMO-to-LUMO excitation and (**b**) HOMO-to-LUMO + 2 excitation. Solid lines and dotted lines are associated with occupied states and empty states, respectively. The red lines indicate time-evolving energy levels of the initial HOMO and (**a**) LUMO [(**b**) LUMO + 2] states. Internal conversion to the electronic ground state happens within 50 fs in both cases.

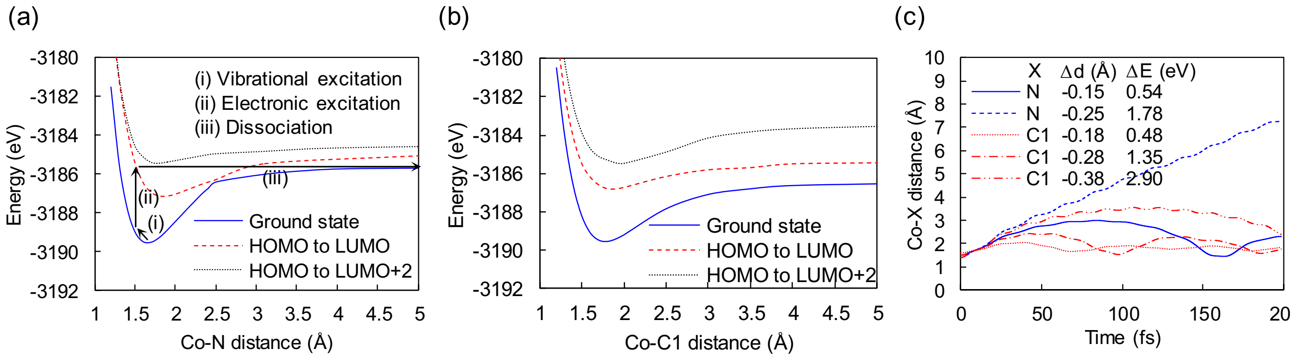

Figure 5. Ligand dissociation induced by a combination of vibrational and electronic excitations. (**a**) Adiabatic potential energy curves as functions of Co–N distance. Arrows with descriptions (i–iii) are associated with a possible pathway of Co–N dissociation induced by HOMO-to-LUMO excitation. (**b**) Adiabatic potential energy curves as functions of Co–C1 distance. (**c**) Time evolution of Co-X distance during coupled electron–ion dynamics initiated by HOMO-to-LUMO excitation. Before the excitation, Co-X distance is initially adjusted by Δd, and the molecule gains energy by ΔE, which is regarded as vibrational excitation at the electronic ground state.

HOMO-to-LUMO + 2 excitation (Fig. 4b), the state is rapidly converted into the S_1, which seems to be consistent with Kasha's rule; however, the short lifetime of S_1 implies breaking Kasha's rule as well.

In the TDDFT-MD, forces exerted on ions are derived using the Ehrenfest dynamics scheme, which is valid in the absence of the mean-field average of PESs. To avoid mixing of PESs, the energy difference between PESs is required to be large enough, which is observed during most of the time of excited-state dynamics of $Co(CO)_3NO$. Figure 4 shows that the occupied orbital energy level originally higher goes down while the empty orbital energy level goes up, where those two levels get close for a short time less than 10 fs. Therefore, except for this short period, the motion of ions is primarily described in a single PES; eventually, after 50 fs, the electronic ground state governs the system. The validation we made for the Ehrenfest dynamics has also been discussed in excited carrier dynamics of carbon nanotubes and in photoisomerization of azobenzene[38,43–45]. As demonstrated above, the Ehrenfest dynamics allows us to perform on-the-fly simulations of the particular system without considering trajectory-based methods, such as fewest-switches surface hopping[56] although the subtle quantum nature of ion dynamics remains elusive. Regarding the zero-point motion[30,40], which is neglected in the classical picture, will be insignificant because the ion temperature is 300 K or higher.

Potential energy curves and vibration-excitation processs. Sobell et al. have demonstrated experimentally that the electron beam facilitates ligand dissociation, which cannot be explained by a typical thermal activation due to substrate heating but can be explained by electronic excitation[4]. Nevertheless, our results so far do not show any instantaneous ligand dissociation. For further investigation, we computed potential energy curves as functions of Co–N and Co-C1 distances (Fig. 5a,b). Based on the potential energy curves, a possible instantaneous dissociation pathway of the NO ligand on the precursor is depicted in Fig. 5a: (i) the Co–N bond is vibrationally excited, (ii) once the bond gains sufficient vibrational energy, electronic excitation is introduced

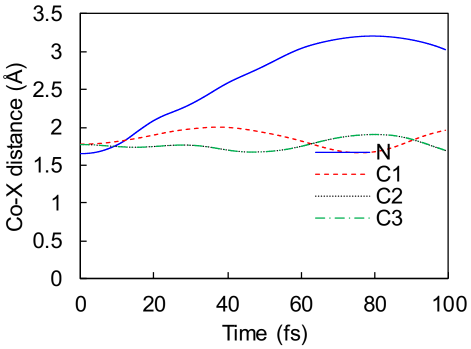

Figure 6. Co–N bond breaking driven by a two-electron excitation from the HOMO to the LUMO. This excitation can be achieved during electron-Co(CO)$_3$NO scattering[57,58].

along with the Franck–Condon principle, and (iii) the system evolves in time and overcomes the dissociation limit. It is worth noting that from the small gap at the crossing point in the adiabatic representation shown in Fig. 5a, a crossing of potential energy curves of the ground state and the HOMO-to-LUMO excited state is expected to be observed in the diabatic representation. Thus, a transition from the first excited state to the ground state can readily occur during the time evolution, which reduces the energy required for the dissociation; however, the barrier is still too high to see dissociation at room temperature without initial vibrational excitation. Comparing bond energies of Co–N and Co-C1 in the ground state shown in Fig. 5a,b, the bond energy of Co–N is greater than that of Co–C1, indicating that the Co–N bond seems to be more difficult to break. Interestingly, electronic excitation can make Co–N break more easily than Co–C1. Figure 5c shows time evolutions of interatomic distances starting with vibrational excitations followed by electronic excitation. The result implies that Co–N bond breaking is more frequent as the thermal energy required for Co–N bond breaking is smaller than that of Co–C1 bond breaking. Through intramolecular vibrational energy redistribution, some electronic excitations can be converted to vibrational energy, which can cause molecular heating sufficient to realize the proposed dissociation even at room temperature; however, the barrier is still too high to see dissociation at room temperature without initial vibrational excitation. This combined process illustrates the stimulated ligand dissociation, which cannot be explained solely by either electronic excitation or thermal activation.

Two-electron process. Another scenario of the electronic-excitation-driven dissociation can involve a two-electron process. In our previous work, we have studied the electron-Co(CO)$_3$NO scattering process for the EE-ALD using the TDDFT[57,58]. It has turned out that the maximum energy transferred from the incident electron wave packet to the molecule can reach approximately 10 eV when the kinetic energy of the incident electron is around 170 eV, which is within the typical energy range used for the EE-ALD[4]. Since the HOMO–LUMO gap is 3.1 eV, the excitation energy of the 10 eV is sufficient to promote two electrons from the HOMO to the LUMO. The two-electron excitation is less likely to happen right after the electron-molecule collision. Having transferred sufficient energy to the molecule, however, the additional excited electron can be generated as in the multiple exciton generation[59,60]. Also, two-electron excitation can be induced by the Knotek-Feibelman mechanism, in which secondary Auger electrons play a leading role in further excitation of the surface molecule[61]. Consecutive scatterings by two electrons or two photons can also be considered as a source of the two-electron excitation. The detailed mechanism and quantitative analysis for the two-electron excitation processes mentioned above could further legitimate the proposed mechanism, albeit beyond the scope of this study.

The employed real-time adiabatic TDDFT can include double excitation with a superposition state, whereas the linear-response adiabatic TDDFT is incapable of dealing with multielectron excited states[62,63]. As a result of TDDFT-MD simulation starting with the two-electron HOMO-to-LUMO excitation, the Co–N bond breaks instantaneously (Fig. 6), which brings about rapid dissociation before the substate or molecule heating. Although the Co–N bond is not fully broken in Fig. 6, the broad amplitude of the band length indicates that a small amount of additional thermal energy or interaction with other molecules can readily cause dissociation. Also, the Co–C1 bond length exhibits a different time evolution from Co–C2 and Co–C3 because of the Co–C1 bonding character different from others, as shown in Fig. 2e, where the N–Co–C1, N–Co–C2, and N–Co–C3 bond angles are 114.1°, 115.6°, and 115.6°, respectively. Interestingly, the adiabatic PEC shown in Figure S4 does not explain the instantaneous bond breaking of Co–N. Accordingly, nonadiabatic coupling can play a crucial role in the dissociation process induced by the two-electron excitation displayed in Fig. 6. However, in contrast to the constrained DFT[64], our typical DFT has a limitation in describing charge or spin localized state when we construct an adiabatic potential energy curve. Therefore, the charge or spin localized state can also play a role in the instantaneous dissociation. Although we could not identify the detailed mechanism because of the limitation of our approach, it remains valid that the Co–N bond breaking can be induced by the two-electron excitation.

Conclusion

In conclusion, using the Ehrenfest-TDDFT method, we investigated the microscopic details of $Co(CO)_3NO$ dissociation driven by electronic excitation and demonstrated two direct dissociation pathways of the NO ligand on the $Co(CO)_3NO$. According to the first dissociation pathway, molecular vibration plays a vital role in the electronic-excitation-driven dissociation. Whereas either single-electron excitation or simple vibrational heating rarely gives rise to ligand dissociation, we found a direct dissociation pathway of the NO ligand on the $Co(CO)_3NO$ by introducing subsequent electronic excitation after vibrational excitation. Another instantaneous dissociation pathway was demonstrated along with a two-electron excitation, which can be induced by energy transferred from an incident electron to the molecule via the electron-molecule scattering. In those dissociation pathways, the CO ligand is less likely to dissociate from the $Co(CO)_3NO$ than the NO ligand although the Co–N has larger bond energy than Co–C in the ground state. However, further experimental and theoretical efforts are necessary to confirm the proposed pathways. In particular, an in-depth investigation of temperature-dependent growth rates in tandem with electronic excitations would allow one to differentiate the effects of vibrational and electronic excitations on ligand dissociation. Also, sophisticated simulation approaches in determining the two-electron excitation process could shed additional light on the proposed mechanism.

Received: 26 January 2021; Accepted: 23 March 2021

References

1. Salahuddin, S., Ni, K. & Datta, S. The era of hyper-scaling in electronics. *Nat. Electron.* **1**, 442–450 (2018).
2. Sprenger, J. K. *et al.* Electron-enhanced atomic layer deposition of boron nitride thin films at room temperature and 100 °C. *J. Phys. Chem. C* **122**, 9455–9464 (2018).
3. Sprenger, J. K., Sun, H., Cavanagh, A. S. & George, S. M. Electron-enhanced atomic layer deposition of silicon thin films at room temperature. *J. Vac. Sci. Technol. A* **36**, 01A118 (2018).
4. Sobell, Z. C., Cavanagh, A. S. & George, S. M. Growth of cobalt films at room temperature using sequential exposures of cobalt tricarbonyl nitrosyl and low energy electrons. *J. Vac. Sci. Technol., A* **37**, 060906 (2019).
5. Utke, I., Hoffmann, P. & Melngailis, J. Gas-assisted focused electron beam and ion beam processing and fabrication. *J. Vac. Sci. Technol. B Microelectron. Nanometer Struct. Process. Meas. Phenomena* **26**, 1197–1276 (2008).
6. Mont, F. W. *et al.* Cobalt interconnect on same copper barrier process integration at the 7nm node. in *2017 IEEE International Interconnect Technology Conference (IITC)* 1–3 (IEEE, 2017). doi:https://doi.org/10.1109/IITC-AMC.2017.7968971.
7. Ervin, M. H. & Nichols, B. M. Electron beam induced deposition of cobalt for use as single- and multiwalled carbon nanotube growth catalyst. *J. Vac. Sci. Technol. B* **27**, 2982 (2009).
8. Gazzadi, G. C. *et al.* Focused electron beam deposition of nanowires from cobalt tricarbonyl nitrosyl ($Co(CO)_3NO$) precursor. *J. Phys. Chem. C* **115**, 19606–19611 (2011).
9. Rosenberg, S. G., Barclay, M. & Fairbrother, D. H. Electron beam induced reactions of adsorbed cobalt tricarbonyl nitrosyl (Co(CO)3NO) molecules. *J. Phys. Chem. C* **117**, 16053–16064 (2013).
10. Vollnhals, F. *et al.* Electron-beam induced deposition and autocatalytic decomposition of $Co(CO)_3NO$. *Beilstein J. Nanotechnol.* **5**, 1175–1185 (2014).
11. Engmann, S., Stano, M., Matejčík, Š & Ingólfsson, O. The role of dissociative electron attachment in focused electron beam induced processing: A case study on cobalt tricarbonyl nitrosyl. *Angew. Chem. Int. Ed.* **50**, 9475–9477 (2011).
12. Engmann, S. *et al.* Absolute cross sections for dissociative electron attachment and dissociative ionization of cobalt tricarbonyl nitrosyl in the energy range from 0 eV to 140 eV. *J. Chem. Phys.* **138**, 044305 (2013).
13. Papp, P. *et al.* An experimental and theoretical study on structural parameters and energetics in ionization and dissociation of cobalt tricarbonyl nitrosyl. *Int. J. Mass Spectrom.* **356**, 24–32 (2013).
14. Thorman, R. M., Kumar, T. P., Fairbrother, D. H. & Ingólfsson, O. The role of low-energy electrons in focused electron beam induced deposition: four case studies of representative precursors. *Beilstein J. Nanotechnol.* **6**, 1904–1926 (2015).
15. Postler, J. *et al.* Electron-induced chemistry of cobalt tricarbonyl nitrosyl ($Co(CO)_3NO$) in liquid helium nanodroplets. *J. Phys. Chem. C* **119**, 20917–20922 (2015).
16. Georgiou, S. & Wight, C. A. Photofragment spectroscopy of cobalt tricarbonylnitrosyl and its trialkylphosphine derivatives. *J. Chem. Phys.* **90**, 1694–1700 (1989).
17. Prinslow, D. A., Niles, S., Wight, C. A. & Armentrout, P. B. Multiphoton ionization of cobalt atoms produced by multiphoton dissociation of Co(CO)3NO and Co(CO)2(NO)PR3 (R=CH3, n-C3H7 and n-C4H9). *Chem. Phys. Lett.* **168**, 482–488 (1990).
18. Bartz, J. A. *et al.* Energy disposal in the photodissociation of $Co(CO)_3NO$ near 225 nm. *J. Phys. Chem. A* **102**, 10697–10702 (1998).
19. Bartz, J. A. *et al.* NO ($v'' = 0$) rotational distributions from the photodissociation of organometallic nitrosyls in the charge transfer region. *J. Phys. Chem. A* **105**, 319–324 (2001).
20. Nakata, H., Nagamori, K., Yamasaki, K. & Kohguchi, H. Detection of direct NO ligand loss in the ultraviolet photodissociation of Co(CO)3NO. *Chem. Phys. Lett.* **707**, 150–153 (2018).
21. Hohenberg, P. & Kohn, W. Inhomogeneous electron gas. *Phys. Rev.* **136**, B864–B871 (1964).
22. Kohn, W. & Sham, L. J. Self-consistent equations including exchange and correlation effects. *Phys. Rev.* **140**, A1133–A1138 (1965).
23. Born, M. & Oppenheimer, R. Zur Quantentheorie der Molekeln. *Ann. Phys.* **389**, 457–484 (1927).
24. Runge, E. & Gross, E. K. U. Density-functional theory for time-dependent systems. *Phys. Rev. Lett.* **52**, 997–1000 (1984).
25. Maitra, N. T. Perspective: Fundamental aspects of time-dependent density functional theory. *J. Chem. Phys.* **144**, 220901 (2016).
26. Li, X., Tully, J. C., Schlegel, H. B. & Frisch, M. J. Ab initio Ehrenfest dynamics. *J. Chem. Phys.* **123**, 084106 (2005).
27. Parandekar, P. V. & Tully, J. C. Mixed quantum-classical equilibrium. *J. Chem. Phys.* **122**, 094102 (2005).
28. Meng, S. & Kaxiras, E. Real-time, local basis-set implementation of time-dependent density functional theory for excited state dynamics simulations. *J. Chem. Phys.* **129**, 054110 (2008).
29. Tritsaris, G. A., Vinichenko, D., Kolesov, G., Friend, C. M. & Kaxiras, E. Dynamics of the photogenerated hole at the rutile TiO_2 (110)/water interface: A nonadiabatic simulation study. *J. Phys. Chem. C* **118**, 27393–27401 (2014).
30. Kolesov, G., Kaxiras, E. & Manousakis, E. Density functional theory beyond the Born–Oppenheimer approximation: Accurate treatment of the ionic zero-point motion. *Phys. Rev. B* **98**, 2 (2018).
31. Kolesov, G., Vinichenko, D., Tritsaris, G. A., Friend, C. M. & Kaxiras, E. Anatomy of the photochemical reaction: Excited-state dynamics reveals the C–H acidity mechanism of methoxy photo-oxidation on titania. *J. Phys. Chem. Lett.* **6**, 1624–1627 (2015).
32. Kolesov, G., Grånäs, O., Hoyt, R., Vinichenko, D. & Kaxiras, E. Real-time TD-DFT with classical ion dynamics: Methodology and applications. *J. Chem. Theory Comput.* **12**, 466–476 (2016).

33. Soler, J. M. *et al.* The SIESTA method for ab initio order-N materials simulation. *J. Phys.: Condens. Matter.* **14**, 2745–2779 (2002).
34. Perdew, J. P., Burke, K. & Ernzerhof, M. Generalized gradient approximation made simple. *Phys. Rev. Lett.* **77**, 3865–3868 (1996).
35. Sawyer, K. R. *et al.* Direct observation of photoinduced bent nitrosyl excited-state complexes. *J. Phys. Chem. A* **112**, 8505–8514 (2008).
36. Troullier, N. & Martins, J. L. Efficient pseudopotentials for plane-wave calculations. *Phys. Rev. B* **43**, 1993–2006 (1991).
37. Wang, H. *et al.* The role of collective motion in the ultrafast charge transfer in van der Waals heterostructures. *Nat. Commun.* **7**, 11504 (2016).
38. Miyamoto, Y., Tateyama, Y., Oyama, N. & Ohno, T. Conservation of the pure adiabatic state in Ehrenfest dynamics of the photoisomerization of molecules. *Sci. Rep.* **5**, 18220 (2015).
39. Parandekar, P. V. & Tully, J. C. Detailed balance in Ehrenfest mixed quantum-classical dynamics. *J. Chem. Theory Comput.* **2**, 229–235 (2006).
40. Horsfield, A. P., Bowler, D. R., Fisher, A. J., Todorov, T. N. & Sánchez, C. G. Beyond Ehrenfest: Correlated non-adiabatic molecular dynamics. *J. Phys.: Condens. Matter.* **16**, 8251–8266 (2004).
41. Rizzi, V., Todorov, T. N., Kohanoff, J. J. & Correa, A. A. Electron-phonon thermalization in a scalable method for real-time quantum dynamics. *Phys. Rev. B* **93**, 024306 (2016).
42. Bang, J., Sun, Y. Y., Liu, X.-Q., Gao, F. & Zhang, S. B. Carrier-multiplication-induced structural change during ultrafast carrier relaxation and nonthermal phase transition in semiconductors. *Phys. Rev. Lett.* **117**, 126402 (2016).
43. Miyamoto, Y., Rubio, A. & Tománek, D. Real-time Ab initio simulations of excited carrier dynamics in carbon nanotubes. *Phys. Rev. Lett.* **97**, 126104 (2006).
44. Miyamoto, Y. Femtosecond electron-ion dynamics in excited nano-materials: Real-time propagation based on the time-dependent density functional theory. *Phys. Status Solidi* **204**, 1925–1930 (2007).
45. Miyamoto, Y. & Rubio, A. Application of the real-time time-dependent density functional theory to excited-state dynamics of molecules and 2D materials. *J. Phys. Soc. Jpn.* **87**, 041016 (2018).
46. Görling, A. Density-functional theory beyond the Hohenberg-Kohn theorem. *Phys. Rev. A* **59**, 3359–3374 (1999).
47. Gavnholt, J., Olsen, T., Engelund, M. & Schiøtz, J. Δ self-consistent field method to obtain potential energy surfaces of excited molecules on surfaces. *Phys. Rev. B* **78**, 075441 (2008).
48. Hedberg, K., Hedberg, L., Hagen, K., Ryan, R. R. & Jones, L. H. Structure and bonding in transition-metal carbonyls and nitrosyls. 2. Gas-phase electron diffraction reinvestigation of tricarbonylnitrosylcobalt. *Inorg. Chem.* **24**, 2771–2774 (1985).
49. Gong, X., Li, Q.-S., Xie, Y., King, R. B. & Schaefer, H. F. III. Mononuclear and binuclear cobalt carbonyl nitrosyls: Comparison with isoelectronic nickel carbonyls. *New J. Chem.* **33**, 2090 (2009).
50. Cooper, G., Sze, K. H. & Brion, C. E. Core and valence-shell electronic excitation of nickel tetracarbonyl by high-resolution electron energy loss spectroscopy. *J. Am. Chem. Soc.* **111**, 5051–5058 (1989).
51. Ziegler, T., Rauk, A. & Baerends, E. J. On the calculation of multiplet energies by the hartree-fock-slater method. *Theoret. Chim. Acta* **43**, 261–271 (1977).
52. Cramer, C. J., Dulles, F. J., Giesen, D. J. & Almlöf, J. Density functional theory: excited states and spin annihilation. *Chem. Phys. Lett.* **245**, 165–170 (1995).
53. Ess, D. H., Johnson, E. R., Hu, X. & Yang, W. Singlet–triplet energy gaps for diradicals from fractional-spin density-functional theory. *J. Phys. Chem. A* **115**, 76–83 (2011).
54. Kasha, M. Characterization of electronic transitions in complex molecules. *Discuss. Faraday Soc.* **9**, 14 (1950).
55. Guo, Y., Bhattacharya, A. & Bernstein, E. R. Ultrafast S_1 to S_0 internal conversion dynamics for dimethylnitramine through a conical intersection. *J. Phys. Chem. A* **115**, 9349–9353 (2011).
56. Tully, J. C. Molecular dynamics with electronic transitions. *J. Chem. Phys.* **93**, 1061–1071 (1990).
57. Lee, Y., Yao, X., Fischetti, M. V. & Cho, K. Real-time ab initio simulation of inelastic electron scattering using the exact, density functional, and alternative approaches. *Phys. Chem. Chem. Phys.* **22**, 8616–8624 (2020).
58. Yao, X., Lee, Y., Ceresoli, D. & Cho, K. First-principles study on electron-induced excitations of ALD precursors: Inelastic electron wave-packet scattering with cobalt tricarbonyl nitrosyl $Co(CO)_3NO$ using time-dependent density functional theory. *Manuscript submitted for publication* (2020).
59. Wolfsberg, M. & Perlman, M. L. Multiple electron excitation in auger processes. *Phys. Rev.* **99**, 1833–1835 (1955).
60. Nozik, A. J. Quantum dot solar cells. *Phys. E* **14**, 115–120 (2002).
61. Gonzalez-Martinez, I. G. *et al.* Electron-beam induced synthesis of nanostructures: A review. *Nanoscale* **8**, 11340–11362 (2016).
62. Maitra, N. T., Zhang, F., Cave, R. J. & Burke, K. Double excitations within time-dependent density functional theory linear response. *J. Chem. Phys.* **120**, 5932–5937 (2004).
63. Isborn, C. M. & Li, X. Modeling the doubly excited state with time-dependent Hartree-Fock and density functional theories. *J. Chem. Phys.* **129**, 204107 (2008).
64. Van Voorhis, T. *et al.* The diabatic picture of electron transfer, reaction barriers, and molecular dynamics. *Annu. Rev. Phys. Chem.* **61**, 149–170 (2010).

Acknowledgements

This work was supported by ASCENT, one of six centers in JUMP, a Semiconductor Research Corporation (SRC) program sponsored by DARPA (Grant No. 2018-JU-2776). This work was also supported by Creative Materials Discovery Program (Grant No. 2015M3D1A1068062) and Nano·Materials Technology Development Program (Grant No. 2016M3A7B4909942) through the National Research Foundation of Korea (NRF) funded by Ministry of Science and ICT. We acknowledge the Texas Advanced Computing Center (TACC) for providing supercomputing resources. We thank Zachary C. Sobell, Prof. Steven George, and Prof. Andrew Kummel for constructive suggestions and discussions.

Author contributions

Y.L. performed the first-principles calculations; Y.L. and G.K. analyzed data. All authors (Y.L., G.K., X.Y., E.K., and K.C.) contributed to the discussion and preparation of the manuscript.

Competing interests

The authors declare no competing interests.

Additional information

Supplementary Information The online version contains supplementary material available at https://doi.org/10.1038/s41598-021-88243-2.

Correspondence and requests for materials should be addressed to K.C.